Journal of Bionic Engineering (2022) 19:1578–1588
https://doi.org/10.1007/s42235-022-00257-2

RESEARCH ARTICLE

Bioinspired Multi-Metal Structures Produced via Direct Ink Writing

Chao Xu[1,2,3] · Xiang Chen[3] · Wenzheng Wu[3] · Qingping Liu[1,2] · Luquan Ren[1,2]

Received: 12 July 2022 / Revised: 26 July 2022 / Accepted: 27 July 2022 / Published online: 25 August 2022

Abstract
Bioinspired Multi-Metal Structures (MMSs) combine distinct properties of multiple materials, benefiting from improved properties and providing superior designs. Additive Manufacturing (AM) exhibits enormous advantages in applying different materials and geometries according to the desired functions at specific locations of the structure, having great potential in fabricating multi-materials structures. However, current AM techniques have difficulty manufacturing 3D MMSs without material cross-contamination flexibly and reliably. This study demonstrates a reliable, fast, and flexible direct ink writing method to fabricate 3D MMSs. The in-situ material-switching system enables the deposition of multiple metallic materials across different layers and within the same layer. 3D Fe–Cu MMSs with complex geometries and fine details are fabricated as proof of concept. The microstructures, chemical and phase compositions, and tensile fracture surfaces of the Fe–Cu interfaces indicate a well-bonded interface without cracks, delamination, or material cross-contamination. We envision this novel method making other metallic combinations and even metal-ceramic components. It paves the way for manufacturing 3D MMSs using AM and establishes the possibilities of numerous MMSs applications in engineering fields.

Keywords Bioinspired · Bionic · Multi-metal structure (MMS) · Direct ink writing (DIW) · Additive manufacturing (AM)

1 Introduction

Creatures in nature have gradually evolved various bio-structures with excellent performance to better adapt to the environment over millions of years. Featuring superior mechanical, optical, electrical, and hydrodynamic properties, these bio-structures inspire the valuable abilities of humans to create and invent. The mouthparts of Humboldt squid are hard and stiff at the tip but relatively soft at another end inside the body. This bio-structure not only enables the mouthparts to easily penetrate the body of the prey but also avoids the reaction force from hurting its own internal organs. Bones consist of dense and stiff cortical bone and light and porous cancellous bone, yielding a stiff and light supporting system. The common ground of these bio-structures is that they combine distinct properties of multiple materials, benefiting from improved properties and providing superior designs.

The manufacturing of multi-materials structures has attracted increasing research attention. However, the traditional manufacturing techniques have difficulties in manufacturing multi-materials structures. Additive Manufacturing (AM) exhibits enormous advantages in applying different materials and geometries according to the desired functions at specific locations of the structure, having great potential in fabricating multi-materials structures [1–3]. However, current AM techniques are limited to manufacturing multi-polymer structures, as polymers are easy to process due to their low melting point and low stiffness. AM of Multi-Metal Structures (MMSs) with superior mechanical properties and heat resistance, which are desired in many engineering fields such as aerospace, biomedical, and automotive industries [4–6], remains a challenge.

The current AM techniques applied in processing 3D MMSs are electrochemical 3D printing [7, 8], direct energy deposition (DED) [9–12], and selective laser melting (SLM)

✉ Chao Xu
chao_xu@jlu.edu.cn

✉ Wenzheng Wu
wzwu@jlu.edu.cn

✉ Qingping Liu
liuqp@jlu.edu.cn

[1] Key Laboratory of Bionic Engineering (Ministry of Education), Jilin University, Changchun 130000, China

[2] Weihai Institute of Bionics, Jilin University, Weihai 264400, China

[3] School of Mechanical and Aerospace Engineering, Jilin University, Changchun 130000, China

[13–18]. Reiser et al. [7] demonstrated the fabrication of Cu–Ag MMSs at the submicron scale via electrohydrodynamic redox 3D printing, which might potentially be applied in small-scale sensors, actuators, and wire bonding. The small processing size and slow printing speed, however, limit the fabrication of mesoscale MMSs that are desirable in most engineering applications. Researchers also attempted to fabricate MMSs via DED, whereas the direct joint of two different metallic materials generates a sharp interface resulting in cracks and delamination due to their distinct thermal properties. Onuike et al. [9] addressed this issue by employing a compositional bond layer (CBL) to bond the two immiscible metallic materials and successfully fabricated crack-free Inconel 718—Ti_6Al_4V bimetallic structures with a Vanadium Carbide CBL. The current DED techniques, however, are limited to producing vertical MMSs, i.e., different materials in different layers but the same material within the same layer, thus not real 3D MMSs. Wei et al. [13] built MMSs using a modified SLM printer with a micro vacuum sucker to remove powders at required locations and ultrasonic dry powder dispensers to deposit the secondary powder. The modified SLM fuses multiple metallic materials across different layers and within the same layer. Nevertheless, the material cross-contamination is unavoidable due to the incomplete powder removal and inaccurate deposition of the secondary powders over the repeated powder spreading and removal processes. Moreover, the material-switching process is complicated and time-consuming, lowering the manufacturing efficiency, especially for 3D MMSs with complex geometries. To summarize, previous scientific publications have rarely reported the fabrication of real 3D MMSs via AM techniques with a reliable and flexible in-situ material-switching system.

To address this issue, this study, for the first time, demonstrates a material extrusion technique, direct ink writing (DIW) [19–25], which can realize the fabrication of 3D MMSs with complex geometries by depositing different metallic materials across different layers and within the same layer. The in-situ material-switching system consists of multiple syringes containing different metallic inks, enabling flexible, fast, and accurate material switching without cross-contamination. Fe and Cu inks are deposited alternately at specific locations according to the digital model to create 3D structures of metal-polymer composites. The as-printed structures are subsequently sintered in a vacuum furnace to achieve Fe–Cu MMSs. The challenge of fabricating MMSs via DIW is the cracks and delamination at the interface due to the mismatch of shrinkage after sintering of different metals. The sintering conditions including temperature, vacuum degree, and sintering duration are investigated and tailored to reach a consistent shrinkage of both metals. This novel method is envisioned to be applicable for other metallic combinations and even metal-ceramic components. It creates a new opportunity for the manufacturing of real 3D MMSs using AM and the possibilities of numerous MMSs applications in engineering fields.

Table 1 Chemical composition of the Fe powder (wt%)

Powder	Fe	O	N	S	C
Fe	Bal	0.112	0.018	0.006	0.003

Table 2 Chemical composition of the Cu powder (wt%)

Powder	Cu	P	O	Sn	Fe
Cu	Bal	0.095	0.058	0.017	0.004

2 Materials and Methods

2.1 Metallic Powders

Pure Fe and Cu powders were purchased from Material Technology Innovations Co. Ltd. and Changsha Tijo Metal Material Co. Ltd., respectively. The chemical compositions of both powders provided by the certificate of conformity are displayed in Tables 1 and 2. Figure 1 presents the scanning electron microscope (SEM) images of Fe and Cu powders and their Particle Size Distributions (PSDs). Both Fe and Cu powders are spherical with a few satellites. The PSDs were characterized using a Bettersize 2600 laser particle size analyzer, showing $D_{10} = 9.5$ µm, $D_{50} = 23.3$ µm, and $D_{90} = 43.4$ µm for the Fe powder and $D_{10} = 16.6$ µm, $D_{50} = 31.5$ µm, and $D_{90} = 50.8$ µm for the Cu powder.

2.2 Metallic Ink Preparation

The binder is a polymer solution prepared by dissolving polylactic acid (PLA, 4032D, Nature works LLC) in dichloromethane (DCM, Tianjin Zhiyuan Chemical Reagent Co. Ltd.) at a weight ratio of 1:4. The solution was rested for 24 h to ensure complete dissolution. The Fe and Cu inks were produced by mixing the corresponding powders with the polymer solution at weight ratios of 3.84:1 and 4.26:1, respectively, using a ball mill mixer (XQM-21, Changsha Tianchuang Powder Technology Co., Ltd.) at a speed of 600 rpm for 1 h to ensure homogenization. Figure 2 depicts the SEM images of the Fe and Cu inks and their thermogravimetric analysis (TGA) results in the atmosphere of N_2. The Fe and Cu powders are wrapped by the polymer binder and are distributed uniformly within the corresponding inks without aggregations. The TGA results indicate that

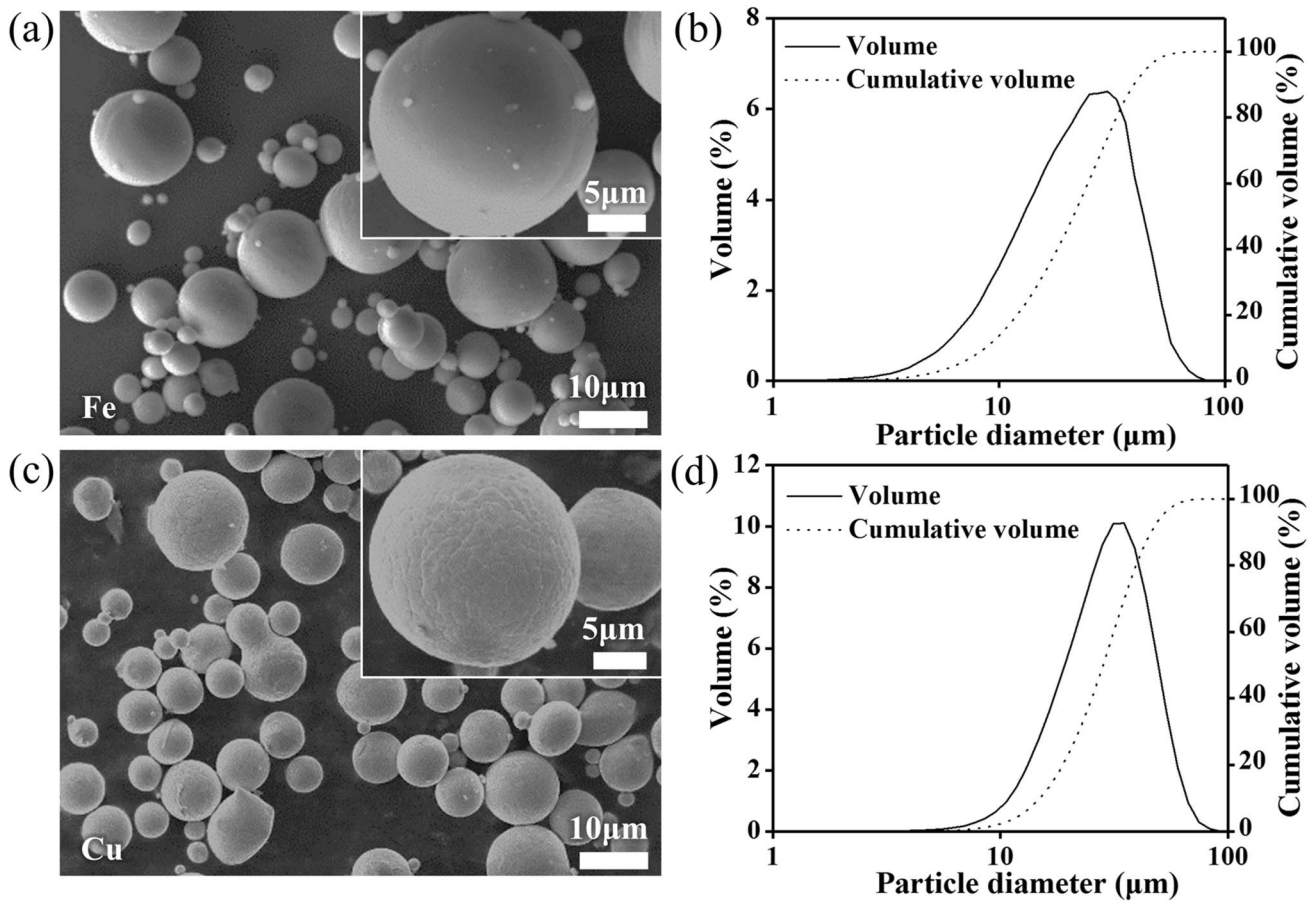

Fig. 1 **a** SEM images and **b** PSD of the Fe powder, **c** SEM images and **d** PSD of the Cu powder

the polymer binder is pyrolyzed under 400 °C in both Fe and Cu inks.

2.3 DIW and Heat-Treatment

Figure 3 presents the schematic and basic setup of the multiple-material DIW 3D printer (AEP-2, Biobond Co. Ltd.) equipped with a computer-controlled 3-axis robot, an air pressure dispensing system, and dual syringes for fabricating MMSs. The digital model was sliced and the G-code was generated by a commercial 3D printing software, simplify 3D. The Fe and Cu inks were loaded in their respective syringes attached with smooth-flow tapered nozzles (Dongguan Tianhong Electronic Technology Co. Ltd., exit inner diameter = 260 μm) for DIW. The metallic inks were extruded at pressures of 0.4–1.0 MPa and the samples were printed at a speed of 18 mm/s. The layer height was set at 80% of the nozzle diameter for better bonding between adjacent layers. The as-printed samples were heat-treated at a vacuum degree of 2 Pa in an alumina tube furnace (LAB Technology, KTL-1700). The samples were sintered at 1025 °C for 6 h with a heating rate of 600 °C/h.

2.4 Analytical Methods

Microstructural characterizations of Fe–Cu interfaces were performed using an SEM (JSM-IT500A, JEOL Beijing co. Ltd.). Chemical and phase compositions of the Fe–Cu interfaces were analyzed via energy-dispersive X-ray spectroscopy (EDS) and X-ray diffraction (XRD, R-AXISRAPID II, Rigaku Smartlab SE), respectively. The cross and longitudinal sectioned samples were prepared by wire cutting, polishing, and subsequent ultrasonic cleaning in absolute ethyl alcohol for 20 min. The uniaxial tensile tests were conducted using a mechanical testing machine (UTM6104) with a 10 kN load cell at a strain rate of 0.04 s^{-1}. The gauge length of tensile bars is 24 mm and the cross-sectional area is 5.5 × 6.0 mm. Five specimens of each sample were tested.

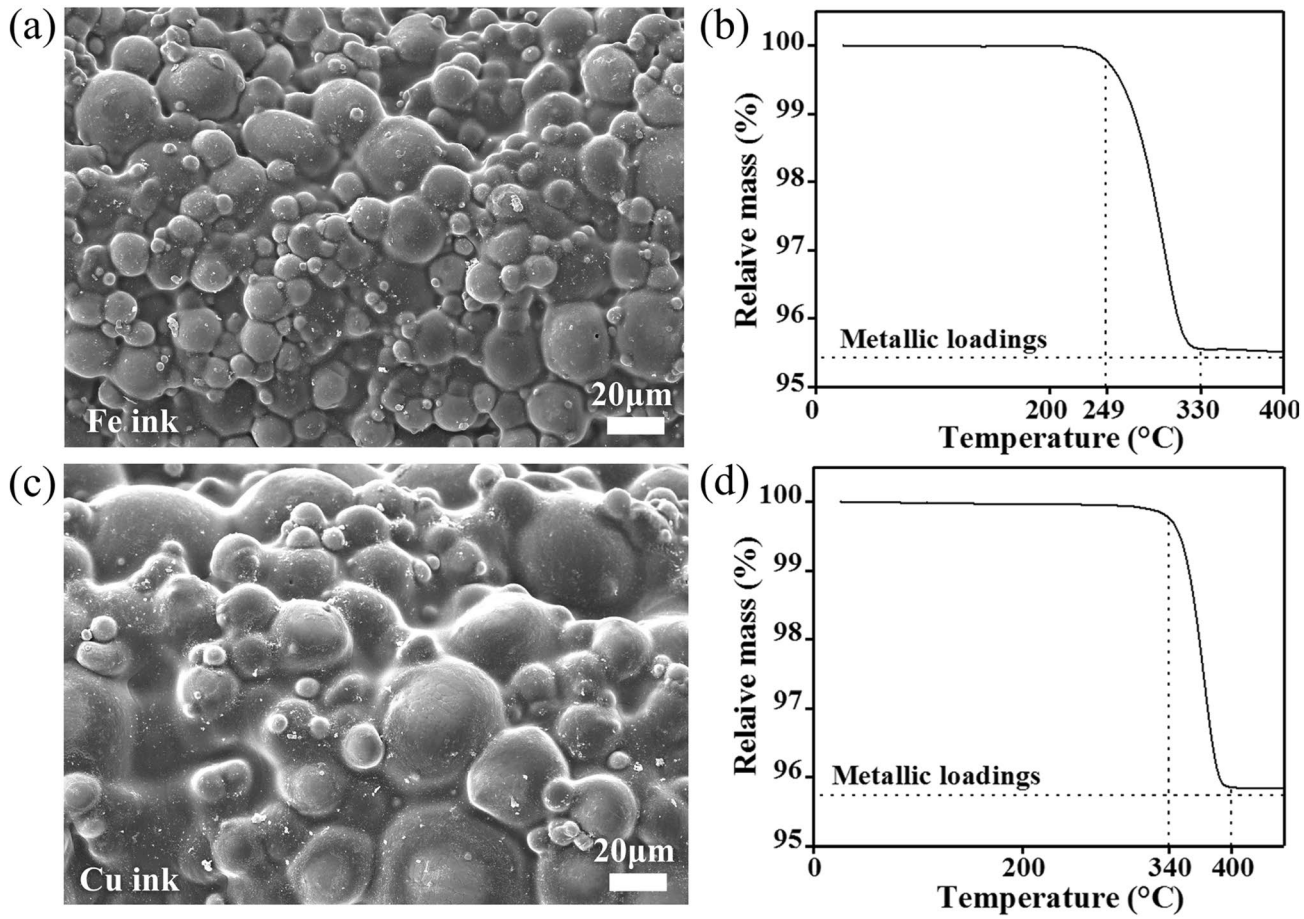

Fig. 2 **a** SEM images and **b** TGA result of the Fe ink, **c** SEM images and **d** TGA result of the Cu ink

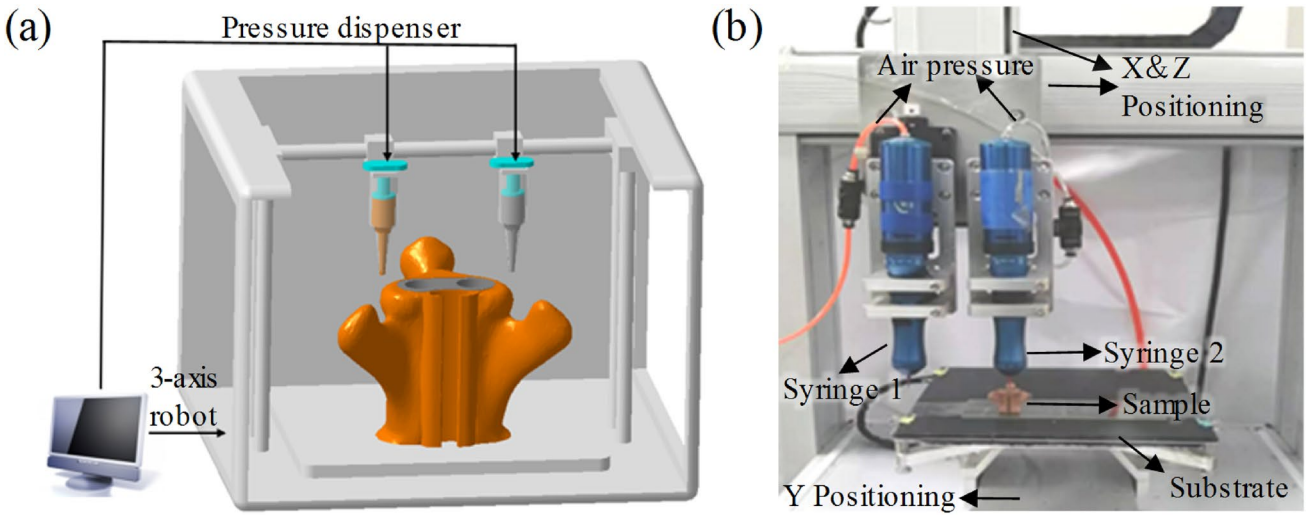

Fig. 3 **a** Schematic and **b** basic setup of the multiple-material DIW 3D printer consisting of duel ink syringes, 3-axis stage and a pressure dispensing system

3 Results and Discussions

3.1 DIW of Fe–Cu Bionic Bones

Figure 4 presents the principle of fabricating a bionic bone consisting of Fe cancellous bone and Cu cortical bone via DIW and subsequent sintering. The DIW process of Fe and Cu inks with the in-situ material-switching system is displayed in Fig. 4a. The syringes loaded with Fe and Cu inks have two states, i.e., "hold" and "extrude", controlled by the pressure dispensing system through "off" and "on" of compressed air, respectively. The two syringes are on "hold" prior to printing (Fig. 4ai). The syringe loaded with Cu ink starts to extrude and deposits Cu ink to the designated locations according to the digital model until all the target areas are finished on the current layer. Meanwhile, the syringe loaded with Fe ink remains on "hold"

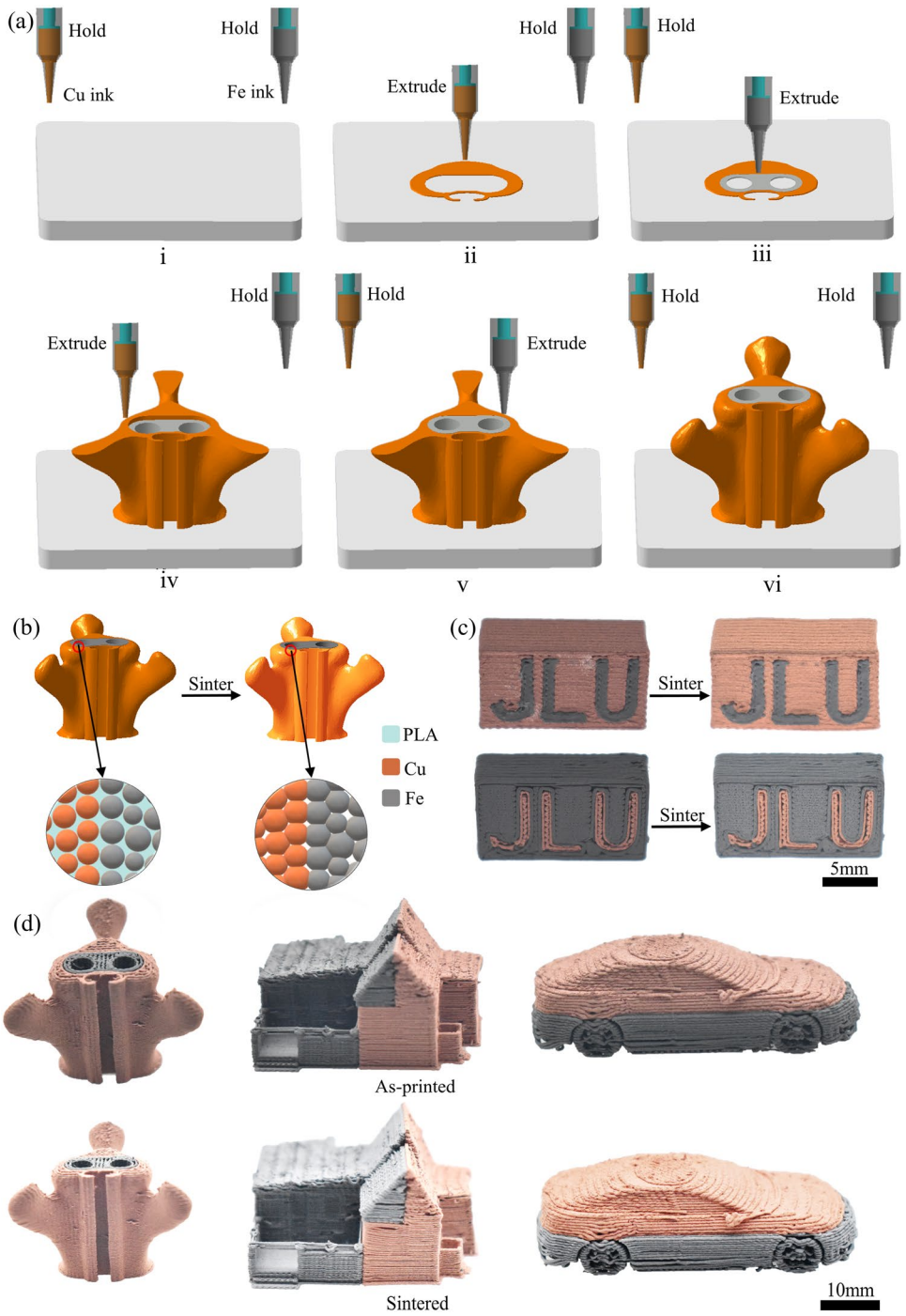

Fig. 4 Schematics of **a** the DIW process of Fe and Cu inks with the in-situ material-switching system, and **b** subsequent sintering of as-printed Fe–Cu bionic bone. **c** As-printed and sintered cuboids embedded with "JLU", the abbreviation for Jilin University. The upper cuboids are made with Fe letters and Cu matrix, and the lower ones are reversed, i.e., Cu letters and Fe matrix. **d** As-printed and sintered Fe–Cu 3D MMS models of a vertebra, a house, and a car

(Fig. 4aii). Subsequently, the two syringes switch states and deposit Fe ink to the designated locations until the Fe part is finished on the current layer, completing the printing of this layer (Fig. 4aiii). The aforementioned processes are repeated layer by layer until the entire Fe–Cu bionic bone is printed, and the two syringes return to "hold" eventually (Fig. 4aiv–vi). The rule of thumb for successful printing is to ensure the same heights of Fe and Cu filaments on the same layer. Thus, the layer heights in the printing program for both inks are set to the same value and identical nozzles are used for both inks. The volatile solvent (DCM) in the ink evaporates right after extrusion, resulting in the shrinkage of the filaments. Thus, the inks are prepared with similar DCM contents to achieve the same filament heights. Based on the results of pre-experiments on different ink formulas and printing parameters, the optimized parameters are applied in this work for successful DIW of Fe–Cu bionic bones.

Figure 4b displays the schematic of subsequent sintering of the as-printed Fe–Cu bionic bones. The metallic powders are embedded and bonded by the polymer binder in the as-printed sample. The polymer binder is pyrolyzed at 400 °C and the structure is held by the friction forces among the adjacent metallic powders. At 1025 °C, the Fe and Cu powders at the interface are fused due to the diffusion of Fe and Cu atoms across the interface, while the nonadjacent Fe and Cu powders are sintered, respectively, achieving a sintered Fe–Cu bionic bone. The challenge of sintering MMSs is the mismatch of shrinkage of different metals after sintering, which might cause cracks and delamination at the interface. The shrinkage is affected by the sintering conditions including temperature, vacuum degree, and sintering duration. The vacuum degree has more influence on structure shrinkage than other factors, especially for Cu due to its high saturation vapor pressure. The sintering conditions were investigated through pre-experiments and were tailored to reach a consistent shrinkage of both metals.

Figure 4c exhibits the as-printed and sintered cuboids embedded with "JLU", the abbreviation for Jilin University. The upper cuboids are made with Fe letters and Cu matrix, and the lower ones are reversed, i.e., Cu letters and Fe matrix. The letters are precisely printed within the matrix material and their interfaces are clear without visible material cross-contamination. Figure 4d shows as-printed and sintered Fe–Cu 3D MMS models of a vertebra, a house, and a car. The 3D MMSs with complex geometries and fine details are successfully printed. The samples preserve their shapes without distortion and material cross-contamination after sintering. The overhang features in the vertebra model are successfully printed without support materials. The metallic inks are designed for optimized printability. Overhang structures with an angle less than 45° can be printed directly without support material. It is rather difficult to fabricate 3D MMSs with complex geometries and different materials intersected in a small building zone, as it leads to more material-switching processes and more possibilities of cracks, delamination, and material cross-contamination at the interfaces. The successful fabrication of Fe–Cu 3D MMSs in Fig. 4c, d, however, demonstrates the flexibility and reliability of this novel DIW method to print multiple metallic materials across different layers and within the same layer, achieving real 3D MMSs with complex geometries and fine details.

3.2 Microstructure, Chemical, and Phase Compositions of the Fe–Cu Interfaces

The quality of the multiple-material interface significantly affects the performance of additive manufactured 3D MMSs. Thus, Fe–Cu interdigital structures with a material intersecting dimension of $5 \times 10 \times 5.4$ mm were fabricated and characterized to investigate the quality of the Fe–Cu interface. Figure 5 shows the as-printed and sintered interdigital structures, microstructures, and chemical compositions at the Fe–Cu interface on the sample surfaces. Figure 5a displays the optical image of the as-printed interdigital structure. The material intersecting region consists of Fe and Cu fingers sandwiched between the interdigital structure, and each finger contains three layers of filaments with a filament diameter of 0.25 mm. The Fe and Cu layer heights of the as-printed sample are the same due to the proper ink formulas and printing parameters, providing a regular structure. The SEM image of the as-printed structure (Fig. 5b) presents magnified details of the Fe–Cu joints where the Fe and Cu powders are wrapped by the polymer binders and are distributed evenly within the corresponding filaments. The Fe and Cu filaments are orderly stacked without significant defects and sharply separated at the interface with null cross-interference. The gaps that appear at the interface are due to the cylindrical shape of the filaments. The EDS results in the map and line-scanning modes indicate that both Fe and Cu were detected only in the respective Fe and Cu zones (Fig. 5c). The noise that occurs in the line-scanning mode is attributed to the interference of the rough surface of the filaments and the polymer cover on the metallic powders. In summary, MMSs with multiple metallic materials across different layers and within the same layer are successfully printed via DIW in the printing stage with null material cross-contamination.

The sintered interdigital structure presents dimensional shrinkage due to the pyrolysis of the polymer binder and the sintering of metallic powders. The Cu part shrinks slightly more than the Fe part, as some Cu powders partially vaporize during sintering due to their relatively higher saturation vapor pressure. The structure preserves its original geometry despite negligible deformation (Fig. 5d). The polymer

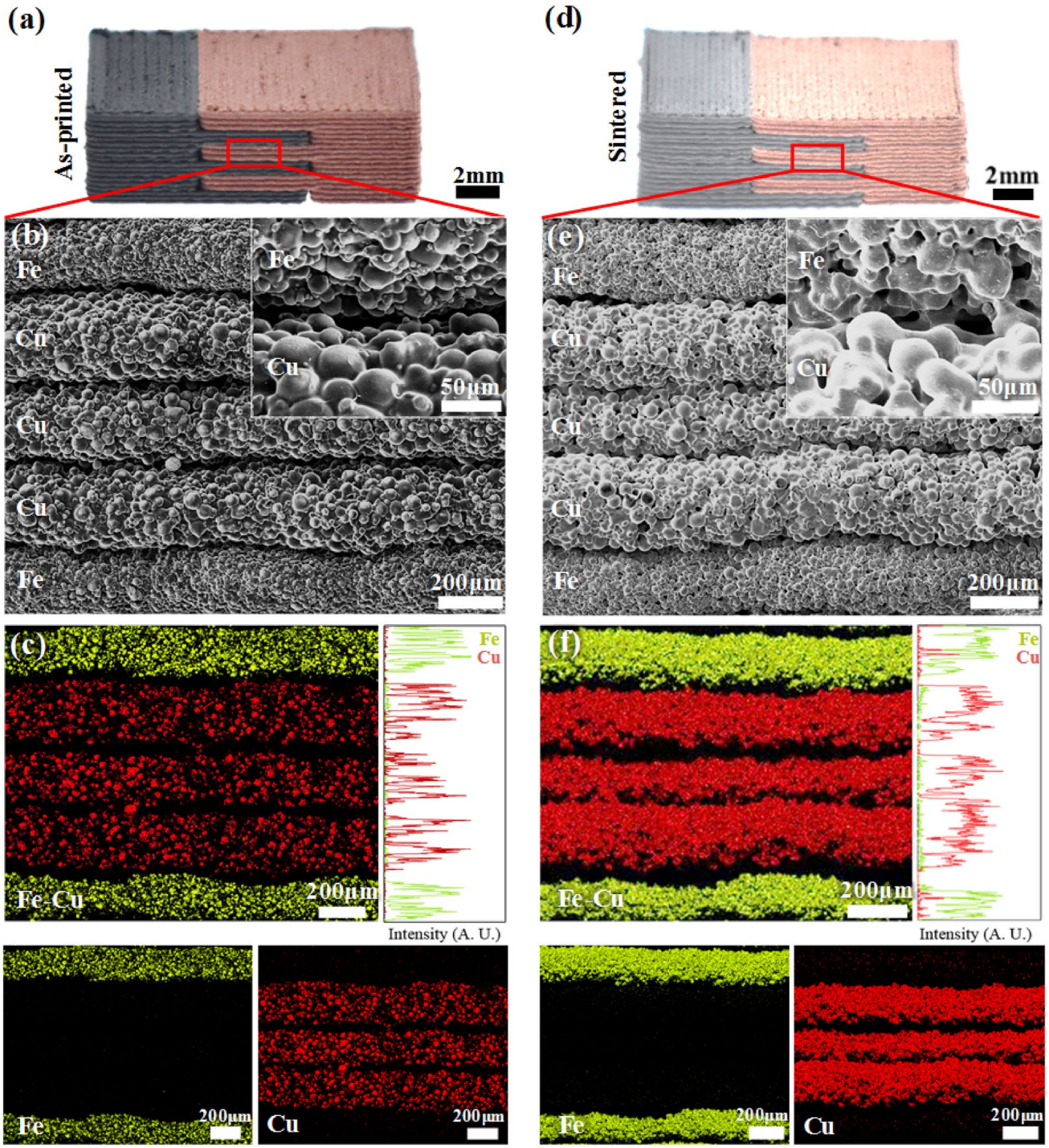

Fig. 5 The surfaces of as-printed and sintered interdigital structures and their Fe–Cu interface characterizations. **a** The optical image, **b** SEM images, and **c** EDS results (Fe in green and Cu in red) of the surface of the as-printed interdigital structure. **d** The optical image, **e** SEM images, and **f** EDS results (Fe in green and Cu in red) of the surface of the sintered interdigital structure

binder disappears and the Fe and Cu powders are sintered. The Fe and Cu powders at the interface are fused through diffusion, while the boundaries are still evident. The sintered filaments are straight and orderly stacked without distortion (Fig. 5e). More Fe and Cu signals appear in EDS due to the disappearance of polymer binder on the surface. Both Fe and Cu were detected only in their respective zones, the same as the as-printed structure (Fig. 5f). Therefore, the sintering does not cause distortion, cracks, delamination, or material cross-contamination.

In addition, the sintered interdigital structures were cut to create cross and longitudinal sections, normal to the building platform, to investigate the internal quality of fabricated MMSs. Figure 6 exhibits the optical images, SEM images, EDS results of the two cutting planes. The optical and SEM images show sharp boundaries between Fe and Cu zones inside the sintered structures (Fig. 6a, b). The inset images in Fig. 6b indicate that Fe and Cu are well bonded at interfaces. The pores and defects on the cutting planes result from the gaps between the cylindrical filaments. More pores and defects that appear on the longitudinal section are attributed to the different printing paths. The noise in the EDS results of the internal structure is less than that of the surfaces because the polished cutting planes are smoother than

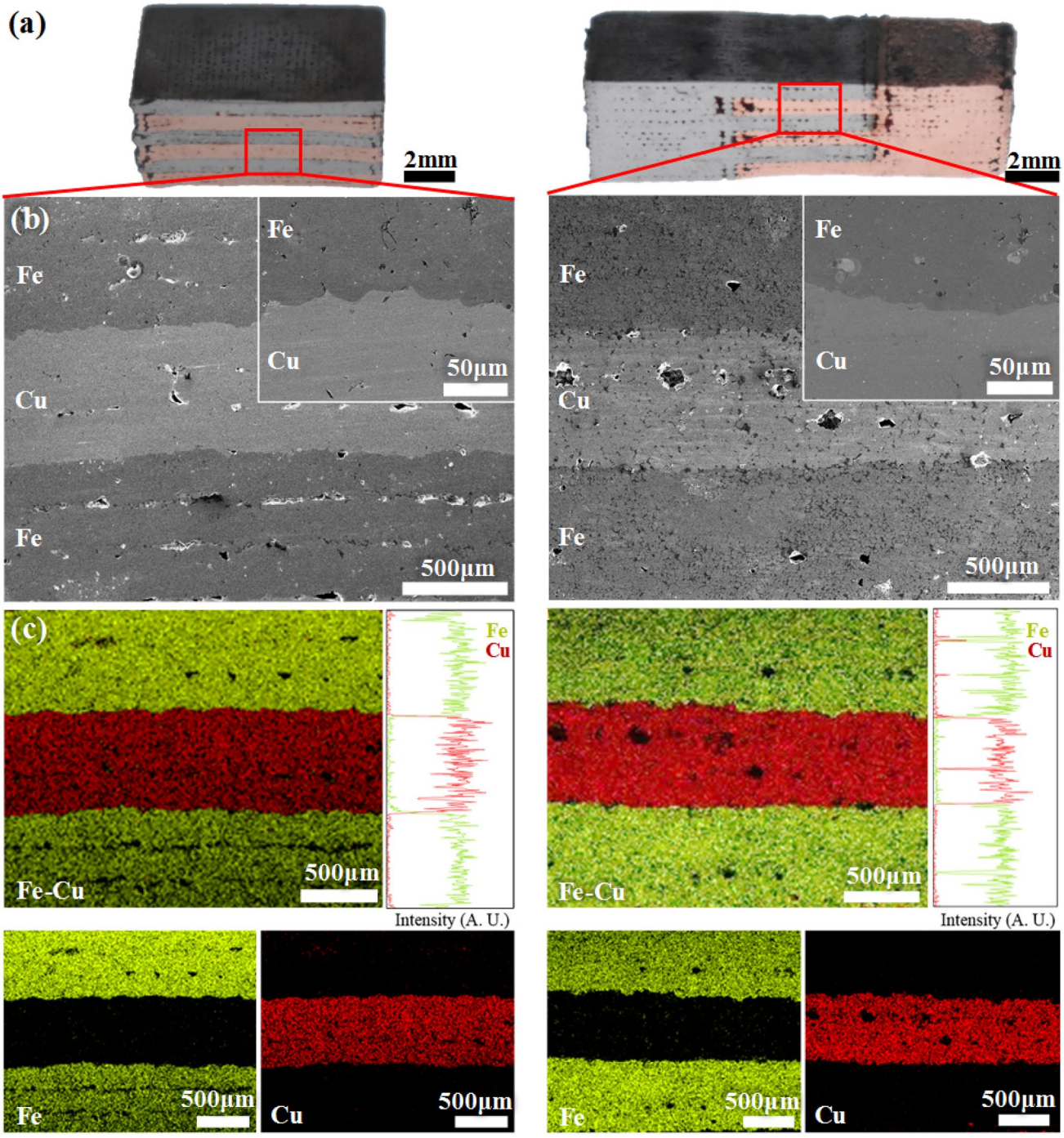

Fig. 6 The cross and longitudinal sections of the sintered interdigital structures and their Fe–Cu interface characterizations. **a** Optical images, **b** SEM images, and **c** EDS results (Fe in green and Cu in red)

the surfaces. The EDS results verify that both Fe and Cu are detected only in their respective zones, which indicates that no material cross-contamination occurred inside the MMS.

The microstructural and chemical composition characterizations on the surface and inside the samples are discussed in detail. DIW with subsequent sintering attests to its capability of precisely deposition different materials across different layers and within the same layers to fabricate MMSs without any cracks, delamination, or material cross-contamination at the interfaces.

Figure 7 presents the XRD results of the raw powders of Fe and Cu, the interfaces between Fe and Cu, and the Fe and Cu zones of the Fe–Cu MMS. The results show that Fe and Cu in the MMS have the same phases as their corresponding raw powders, which indicates that the manufacturing process or the fusion at the interfaces does not change the phase composition of the raw metallic powders.

To investigate the mechanical properties of the MMSs, Fe–Cu, Fe, and Cu tensile bars were fabricated and characterized via uniaxial tensile tests. The Fe–Cu tensile bar has an interdigital length of 10 mm in the middle. The ultimate tensile strength (UTS) of Fe–Cu MMS (53.0 ± 7.5 MPa) is slightly lower than that of Fe (59.7 ± 2.9 MPa) and Cu (56.8 ± 5.4 MPa), as expected. The low UTSs of all the samples are mainly attributed to three reasons. The clues can be tracked in the SEM images of tensile fracture surfaces of the Fe, Cu, and Fe–Cu tensile bars in Fig. 8. First, structural pores and gaps appear between the stacked cylindrical filaments. Second, the filaments have an alternately orthogonal arrangement in the adjacent layers. The layers filled with filaments oriented perpendicular to the tensile direction contribute limited tensile resistance. Third, the relatively low sintering temperature (1025 °C) was set to ensure a similar amount of shrinkage for Fe and Cu, which however results in incomplete fusion of the metallic powders, reducing the tensile properties. Although the UTSs of all the samples are relatively low, the value of Fe–Cu is close to that of Fe and Cu. It implies that Fe and Cu at the interfaces are fused favorably, which is also affirmed by the SEM image of the Fe–Cu tensile fracture surface.

In some cases, the not-so-good mechanical properties are demanded in particular by such applications as artificial bone implants manufacturing. The ideal bone implants should have relatively low mechanical properties to avoid stress shielding and porous structure to facilitate the growth of bone tissues. These porous MMSs produced via DIW fit the mechanical requirements of biomedical applications. Furthermore, the mechanical properties can be improved

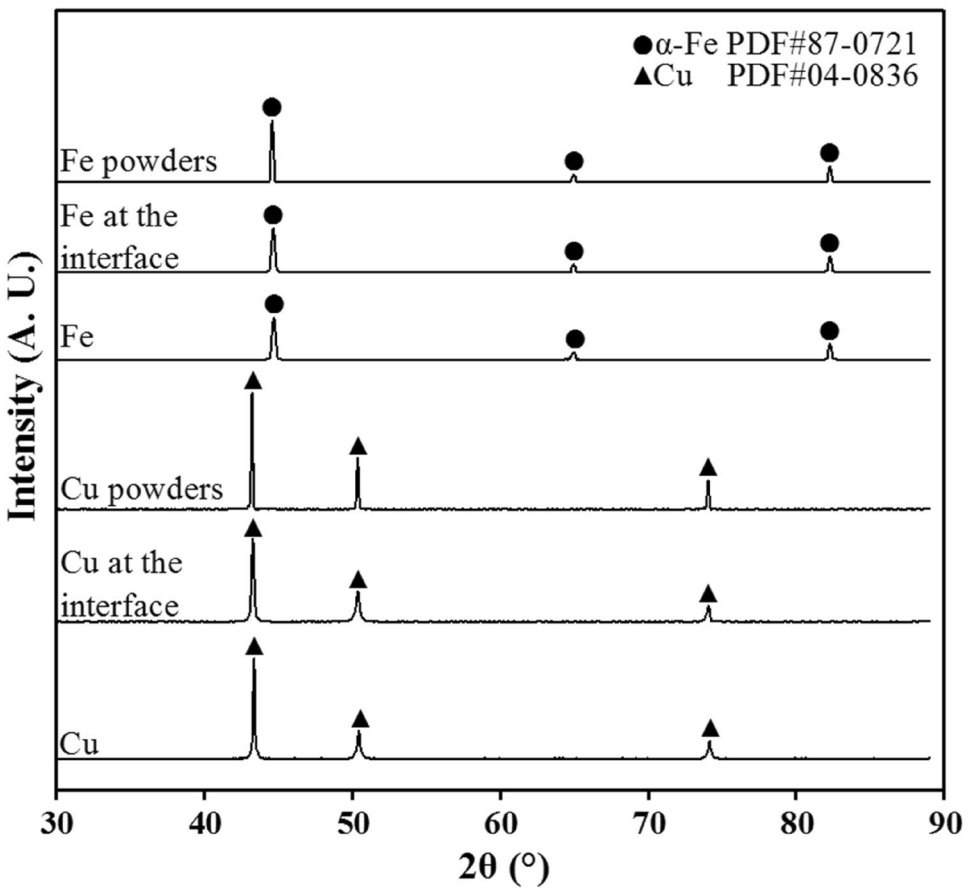

Fig. 7 XRD results of Fe and Cu raw powders, Fe and Cu at interfaces, and Fe and Cu zones of the Fe–Cu MMS

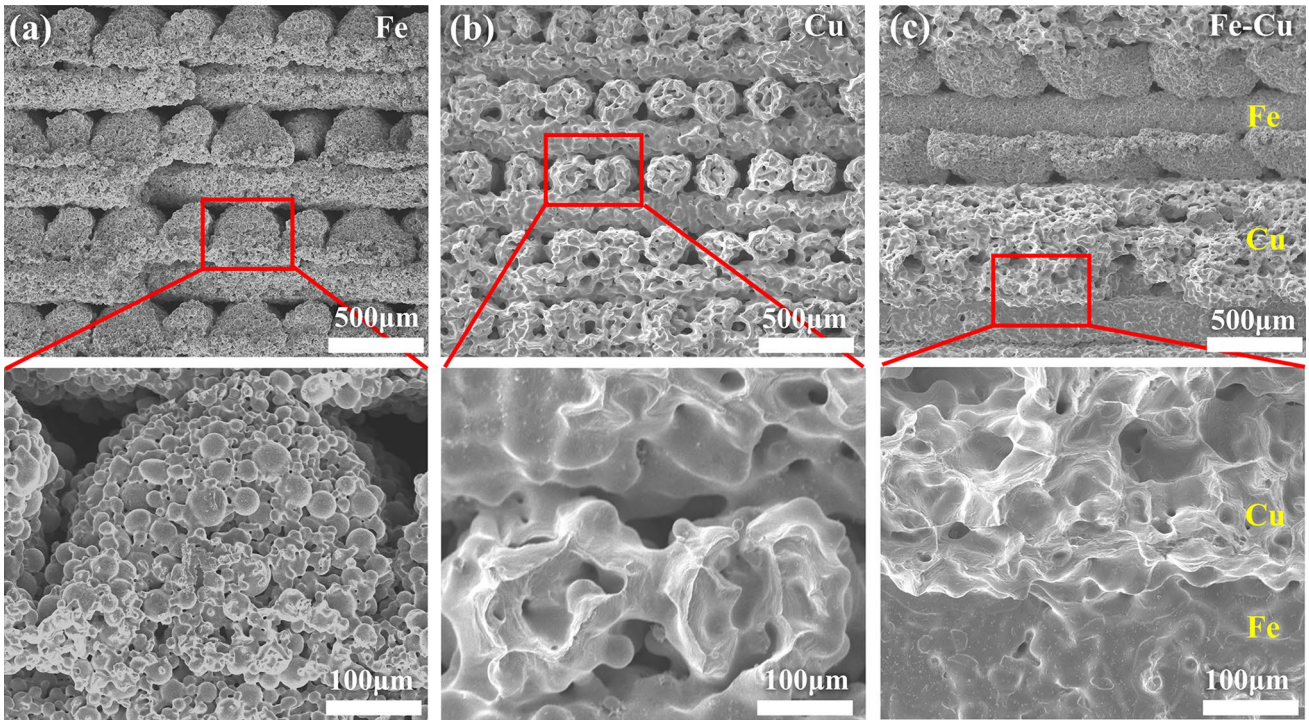

Fig. 8 SEM images of tensile fracture surfaces of the **a** Fe, **b** Cu, and **c** Fe–Cu interdigital structures fabricated via DIW and subsequent sintering

by using nozzles with a rectangular tip to reduce the gaps between filaments, tailoring the printing paths, or optimizing the sintering parameters to enhance the fusion among metallic powders. This would broaden the application fields of DIW produced MMSs to the aerospace and automotive industries.

4 Conclusion

Inspired by the nature, this innovative study, for the first time, employed direct ink writing (DIW) of multiple metallic inks and the subsequent sintering to fabricate real 3D multi-metal structures (MMSs) with complex geometries. An outstanding advantage of the method is the ability to print multiple metallic materials not only within the same layer but also across different layers, which has only been achieved by modified selective laser melting (SLM). Moreover, the flexible and reliable in-site material-switching system with multiple syringes is capable of changing materials arbitrarily with null material cross-contamination, which is difficult for the vacuum sucker and dry powder dispenser in modified SLM. Complicated 3D Fe–Cu MMSs with fine details are successfully fabricated without significant distortion. The microstructures, chemical and phase compositions, tensile fracture surfaces of the Fe–Cu interfaces indicate a well-bonded interface without cracks, delamination, or material cross-contamination. The tensile properties of Fe–Cu MMSs are relatively low due to the gaps between cylindrical filaments, alternately orthogonal arrangement of filaments in adjacent layers, and relatively low sintering temperature. These porous MMSs with relatively low mechanical properties have great potential in manufacturing bone implants in biomedical fields. Our future work will improve the mechanical properties to broaden the application fields of DIW produced MMSs to the aerospace and automotive industries. This novel method is envisioned to be applicable for other metallic combinations and even metal-ceramic components. It creates new opportunities for the manufacturing of bioinspired 3D MMSs using AM and the possibilities of numerous MMSs applications in biomedical and engineering fields.

Acknowledgements The authors are grateful to Prof. Lu Zhang of Jilin University for their constructive feedback on the manuscript.

Author Contributions CX: conceptualization, writing—original draft, writing—review & editing, supervision, project administration, resources, funding acquisition. XC: methodology, investigation, data curation. WW, QL, and LR: supervision.

Funding This work is supported by National Natural Science Foundation of China, China (Grant ID: 52105343 and 52021003), China Postdoctoral Science Foundation, China (Grant ID: 2021M701387 and 2022T150259), and Department of Science and Technology of Jilin Province, China (Grant ID: 2020122214JC).

Data Availability The data used to support the findings of this study are available from the corresponding author upon request.

Declaration

Conflict of interest The authors declare that they have no known competing financial interests or personal relationships that could have appeared to influence the work reported in this paper.

References

1. Ahmed F, Waqas M, Shaikh B, Khan U, Soomro AM, Kumar S, Ashraf H, Memon FH, Choi KH (2022) Multi-material bio-inspired soft octopus robot for underwater synchronous swimming. Journal of Bionic Engineering 19(5).
2. Chan, Y., Tse, Z. T. H., & Ren, H. (2022). Printable Kirigami-inspired flexible and soft anthropomorphic robotic hand. *Journal of Bionic Engineering, 19*(3), 668–677.
3. Men, X., Li, Z., Yang, W., Wang, M., Liang, S., Sun, H., Liu, Z., Lu, G. (2022) 3D-Printed bio-inspired multi-channel cathodes for zinc–air battery applications. Journal of Bionic Engineering, 1–10.
4. Zhang, Y., & Bandyopadhyay, A. (2019). Direct fabrication of bimetallic Ti6Al4V+ Al12Si structures via additive manufacturing. *Additive Manufacturing, 29*, 100783.
5. Bose, S., Vahabzadeh, S., & Bandyopadhyay, A. (2013). Bone tissue engineering using 3D printing. *Materials today, 16*(12), 496–504.
6. Tey, C. F., Tan, X., Sing, S. L., & Yeong, W. Y. (2020). Additive manufacturing of multiple materials by selective laser melting: Ti-alloy to stainless steel via a Cu-alloy interlayer. *Additive Manufacturing, 31*, 100970.
7. Reiser, A., Lindén, M., Rohner, P., Marchand, A., Galinski, H., Sologubenko, A. S., & Spolenak, R. (2019). Multi-metal electrohydrodynamic redox 3D printing at the submicron scale. *Nature Communications, 10*(1), 1–8.
8. Chen, X., Liu, X., Ouyang, M., Chen, J., Taiwo, O., Xia, Y., & Wu, B. (2019). Multi-metal 4D printing with a desktop electrochemical 3D printer. *Scientific Reports, 9*(1), 1–9.
9. Onuike, B., & Bandyopadhyay, A. (2018). Additive manufacturing of Inconel 718–Ti6Al4V bimetallic structures. *Additive Manufacturing, 22*, 844–851.
10. Onuike, B., Heer, B., & Bandyopadhyay, A. (2018). Additive manufacturing of Inconel 718—Copper alloy bimetallic structure using laser engineered net shaping (LENS™). *Additive Manufacturing, 21*, 133–140.
11. Onuike, B., & Bandyopadhyay, A. (2019). Bond strength measurement for additively manufactured Inconel 718-GRCop84 copper alloy bimetallic joints. *Additive Manufacturing, 27*, 576–585.
12. Onuike, B., & Bandyopadhyay, A. (2020). Functional bimetallic joints of Ti6Al4V to SS410. *Additive Manufacturing, 31*, 100931.
13. Wei, C., Li, L., Zhang, X., & Chueh, Y. H. (2018). 3D printing of multiple metallic materials via modified selective laser melting. *CIRP Annals, 67*(1), 245–248.
14. Wei, C., Sun, Z., Huang, Y., & Li, L. (2018). Embedding anti-counterfeiting features in metallic components via multiple material additive manufacturing. *Additive Manufacturing, 24*, 1–12.
15. Wei, C., Sun, Z., Chen, Q., Liu, Z., & Li, L. (2019). Additive manufacturing of horizontal and 3D functionally graded 316L/Cu10Sn components via multiple material selective laser melting. *Journal of Manufacturing Science and Engineering, 141*(8), 081014.
16. Chueh, Y. H., Wei, C., Zhang, X., & Li, L. (2020). Integrated laser-based powder bed fusion and fused filament fabrication for three-dimensional printing of hybrid metal/polymer objects. *Additive Manufacturing, 31*, 100928.
17. Gu, H., Wei, C., Li, L., Han, Q., Setchi, R., Ryan, M., & Li, Q. (2020). Multi-physics modelling of molten pool development and track formation in multi-track, multi-layer and multi-material selective laser melting. *International Journal of Heat and Mass Transfer, 151*, 119458.
18. Xu, C., Sikan, F., Atabay, S. E., Muniz-Lerma, J. A., Sanchez-Mata, O., Wang, X., & Brochu, M. (2020). Microstructure and mechanical behavior of as-built and heat-treated Ti–6Al–7Nb produced by laser powder bed fusion. *Materials Science and Engineering, 793*, 139978.
19. Xu, C., Yu, S., Wu, W., Liu, Q., & Ren, L. (2022). Direct ink writing of Fe bone implants with independently adjustable structural porosity and mechanical properties. *Additive Manufacturing, 51*, 102589.
20. Elsayed, H., Rebesan, P., Giacomello, G., Pasetto, M., Gardin, C., Ferroni, L., & Biasetto, L. (2019). Direct ink writing of porous titanium (Ti6Al4V) lattice structures. *Materials Science and Engineering: C, 103*, 109794.
21. Jakus, A. E., Taylor, S. L., Geisendorfer, N. R., Dunand, D. C., & Shah, R. N. (2015). Metallic architectures from 3D-printed powder-based liquid inks. *Advanced Functional Materials, 25*(45), 6985–6995.
22. Kenel, C., Casati, N. P., & Dunand, D. C. (2019). 3D ink-extrusion additive manufacturing of CoCrFeNi high-entropy alloy micro-lattices. *Nature Communications, 10*(1), 1–8.
23. Xu, C., Quinn, B., Lebel, L. L., Therriault, D., & L'Espérance, G. (2019). Multi-material direct ink writing (DIW) for complex 3D metallic structures with removable supports. *ACS Applied Materials & Interfaces, 11*(8), 8499–8506.
24. Xu, C., Wu, Q., L'Espérance, G., Lebel, L. L., & Therriault, D. (2018). Environment-friendly and reusable ink for 3D printing of metallic structures. *Materials & Design, 160*, 262–269.
25. Xu, C., Bouchemit, A., L'Espérance, G., Lebel, L. L., & Therriault, D. (2017). Solvent-cast based metal 3D printing and secondary metallic infiltration. *Journal of Materials Chemistry C, 5*(40), 10448–10455.